

Quantum chaos of an ion trapped in a linear ion trap

Gennady P. Berman

Theoretical Division T-13, and CNLS, Los Alamos National Laboratory, Los Alamos, New Mexico 87545

Daniel F. V. James

Theoretical Division T-4, Los Alamos National Laboratory, Los Alamos, New Mexico 87545

Dimitri I. Kamenev

Theoretical Division T-13, and CNLS, Los Alamos National Laboratory, Los Alamos, New Mexico 87545 and Nizhny Novgorod State University, Nizhny Novgorod, 603600, Russia

(Received 31 January 2000; accepted for publication 20 March 2000)

We describe the transition to quantum chaos of an ion trapped in a linear ion trap and interacting with two laser fields. Under the conditions of adiabatic illumination of the upper level of the ion, and when the frequencies of the two laser beams are slightly different, the system is reduced to a quantum linear oscillator interacting with a monochromatic wave. The property of localization over the quantum resonance cells is proposed to exploit in order to facilitate the process of measurement of the probability distribution of an ion on the vibrational levels. In the regime of strong chaos the time-averaged values of the energy and dispersion of energy are computed and compared with the corresponding classical quantities for different values of the perturbation amplitude. In the exact resonance case, the classical analog of the system possesses an infinite inhomogeneous stochastic web. We analyze the quantum dynamics inside the inhomogeneous web. It is shown that the quantum system mimics on average the dynamics of the corresponding classical system. Formation of the quantum resonance cells is illustrated in the case of a finite detuning from the exact resonance, and under increasing of the wave amplitude. The parameters of the model and the initial conditions are close to the real physical situation which can be realized in the system of cold trapped ion perturbed by two lasers fields with close frequencies. © 2000 American Institute of Physics. [S1054-1500(00)01502-0]

The transition to quantum chaos is considered in the system of cooled trapped ion perturbed by a monochromatic field of two lasers with close frequencies. This system is important for studying conditions of stable operation in future quantum computer devices. In some region of parameters, the system is reduced to the quantum harmonic oscillator interacting with a monochromatic wave. In the case of the exact resonance, the classical phase space possesses an infinite inhomogeneous stochastic web which separates the classical resonance cells. Inside each cell the classical particles move along regular closed trajectories. When the wave amplitude increases the width of the web also increases. It is shown that chaotization of the phase space leads to increasing the probability of the quantum particle to move from one quantum cell to another. In the regime of strong classical chaos, the time-averaged quantities of the energy and the dispersion of energy behave similarly in both classical and quantum systems. The formation of the quantum resonance cells is demonstrated at finite detuning from the exact resonance and under increasing of the wave amplitude. The results derived in this article can be used for understanding the regions of stability and quantum chaos of an ion in linear ion trap devices.

I. INTRODUCTION

Recently, devices based on trapped ions have been used to investigate experimentally fundamental aspects of quan-

tum mechanics,^{1,2} for important technological applications such as optical frequency standards³ and for quantum computing.^{4,5} An ion trapped in an ion trap is considered as a candidate for realizing quantum logic operations by applying a laser radiation to the internal degrees of freedom of the ion.⁵ When the radiation field is rapidly and periodically switched, this system can be described as a kicked harmonic oscillator.^{6,7} In Ref. 8, a model was proposed in which the trapped ion, perturbed by the field of two laser beams with close frequencies, reduces to the model of a harmonic oscillator interacting with a monochromatic wave. In this article, we analyze in detail a transition to quantum chaos in the model.⁸ The results obtained for the quantum model are compared with the classical dynamics.

As was shown in Ref. 9 the quantum Hilbert space of a harmonic oscillator interacting with a monochromatic wave is divided into the quantum resonance cells. The dynamical manifestation of such a division is the property of localization over the quantum resonance cells. In this case, the probability distribution exponentially drops mainly at the boundaries of the cells—quantum web-tori—being on average the same inside the cells. In this article, we show that with increasing of the wave amplitude, the quantum web-tori become more “penetrating.” This behavior corresponds to increasing of the probability for a quantum particle to travel between the cells due to the increase of the chaotic component in the classical phase space.

The main difference between the classical and quantum systems which possess an infinite homogeneous chaotic web

in the phase space is the phenomenon of dynamical localization. Due to this phenomenon, the quantum systems mimics the dynamics of the corresponding classical analog only during a finite time, after which the quantum interference effects cease the quantum diffusion, while the classical diffusion is not changed. The dynamical localization was observed in the kicked rotor¹⁰ and, under definite conditions, in the kicked oscillator.¹¹ The system considered in this article also possesses an infinite stochastic web, but, unlike the above mentioned models, in our case the web is inhomogeneous—the web's width decreases with increasing the coordinate or momentum. The results of this article show that for large times and in the regime of strong classical chaos no significant difference was observed in the classical and chaotic average dynamics.

The investigated classical system has an infinite stochastic web only in the case of the exact resonance. In any real situation there always is a finite detuning from the exact resonance. The size of the web and the number of the resonant cells in this case depend on the relation between the values of the wave amplitude and the detuning from exact resonance. It is shown that the formation of quantum resonance cells, with increasing the wave amplitude, changes the localization properties of the quantum system. When the wave amplitude is small, we observe localization over the individual levels, which corresponds to absence of the resonant cells in the phase space. In the case when the wave amplitude is large enough, we observe formation of the plateaus in the probability distribution which is specific for the degenerate system. The transition from one type of localization to another is shown to correspond to a formation of the classical resonant cells in the phase space.

Below, in this article, we used a set of parameters and initial conditions which allow an experimental verification of obtained results by using the type of ion trap apparatus currently being used to investigate quantum computation.

The article is organized as follows. In Sec. II the transition to chaos in the classical harmonic oscillator interacting with a monochromatic wave is described. In Sec. III we study how a transition to chaos is manifested in localization properties of the quantum system in the case of exact resonance. Time-averaged values of the energy and the dispersion of energy are compared with the corresponding classical quantities at different values of the wave amplitude and the dimensionless Planck constant. Formation of the quantum resonance cells with increasing the wave amplitude is demonstrated in Sec. IV in the near resonance case. In conclusion we outline the results.

II. CLASSICAL DYNAMICS

The classical dynamics of the harmonic oscillator interacting with a monochromatic wave is described by the Hamiltonian,

$$H = \frac{p^2}{2M} + \frac{M\omega^2}{2}x^2 + \frac{\epsilon}{k}\cos(kx - \Omega t) = H_0 + V(x, t), \quad (1)$$

where M is the mass of the particle, p is the momentum, k is

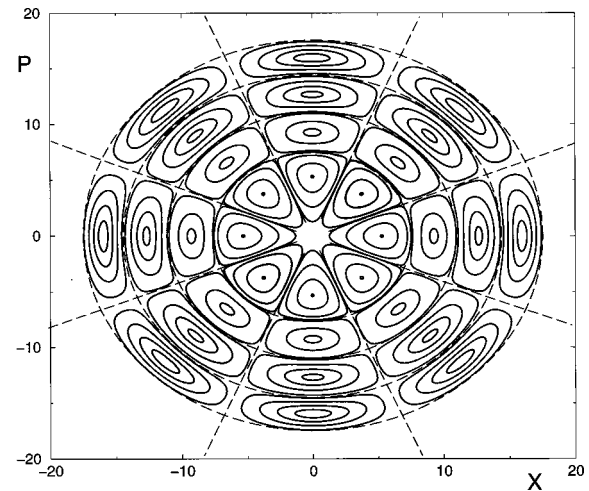


FIG. 1. The classical phase space for the harmonic oscillator in the monochromatic wave field, under the condition of exact resonance: $l=4$, $\epsilon=0.05$. The separatrix net is indicated by the dashed curves.

the wave vector, ϵ/k is the amplitude of the wave, H_0 is the Hamiltonian of the unperturbed harmonic oscillator. In Eq. (1) the same notations as in Ref. 8 are used.

The system, described by Eq. (1), possesses very interesting properties.¹² When the resonant condition is satisfied, $l\omega = \Omega$, $l=1, 2, \dots$, an infinitely small perturbation generates in the classical phase space, an infinite number of resonance cells. The particles move along closed trajectories inside the cells. The resonance cells are separated from each other by the separatrix net. This net is covered by stochastic layers which form the infinite stochastic web. Under the condition of weak chaos, $\epsilon \ll 1$, the web width is negligibly small and almost all classical trajectories are enclosed inside the cells as illustrated in Fig. 1 (case $l=4$). The phase space is shown in the Fig. 1 in the variables (X, P) , where $X=kx$ and $P=kp/M\omega$ are, respectively, the dimensionless coordinate and momentum. The phase space has an axial symmetry of the order $2l$. (In Fig. 1 the separatrix net is indicated by the dashed curves.) A classical ion trapped in a resonant cell remains localized in this cell forever.

It is more convenient to work with ‘‘action-angle’’ variables which can be introduced in the following way. We perform a transformation from the variables (p, x) to the canonically conjugated variables (P_φ, φ) ,

$$x = (2P_\varphi/M\omega)^{(1/2)} \sin \varphi = r(P_\varphi) \sin \varphi, \quad (2)$$

$$p = (2P_\varphi M\omega)^{(1/2)} \cos \varphi = M\omega r(P_\varphi) \cos \varphi, \quad (3)$$

where $r(P_\varphi) = (2P_\varphi/M\omega)^{1/2}$ is the amplitude of oscillations. In these new variables, the Hamiltonian (1) is,

$$H = P_\varphi \omega + P_\beta \Omega + \frac{\epsilon}{k} \cos(kr \sin \varphi - \beta), \quad (4)$$

where $\beta = \Omega t$. Here the variables (P_β, β) are also canonically conjugate. The nonlinear perturbation in Eq. (4) can be expanded in the series,

$$\frac{\epsilon}{k} \cos(kr \sin \varphi - \beta) = \frac{\epsilon}{k} \sum_{n=-\infty}^{\infty} J_n(kr) \cos(n\varphi - \beta). \quad (5)$$

Under the resonance condition, $l\dot{\varphi} = \dot{\beta}$ or $l\omega = \Omega$, all terms in the sum in the right-hand side of Eq. (5) quickly oscillate and can be averaged out, except for one term with $n=l$. In this approximation, the Hamiltonian (4) reduces to,

$$H = \bar{P}_\varphi \omega + \bar{P}_\beta \Omega + \frac{\epsilon}{k} J_l(kr) \cos(l\varphi - \beta). \quad (6)$$

It is convenient to introduce the new resonance variables, (I, θ) , $(\bar{P}_\beta, \tilde{\beta})$, by using the generating function,

$$F = I(l\varphi - \beta) + \bar{P}_\beta \beta.$$

The new Hamiltonian,

$$H = I(l\omega - \Omega) + \bar{P}_\beta \omega + \frac{\epsilon}{k} J_l(kr) \cos \theta, \quad (7)$$

is independent of the variable $\tilde{\beta}$. Hence, $\bar{P}_\beta = \text{const}$. The Hamiltonian,

$$\tilde{H} = H - \bar{P}_\beta \omega = I\delta\omega + \frac{\epsilon}{k} J_l(kr) \cos \theta, \quad (8)$$

where $\delta = l - \Omega/\omega$, is called the ‘‘resonance Hamiltonian.’’¹² It is independent of time, unlike the initial Hamiltonian (1), and mainly determines the motion along the closed regular trajectories inside the resonance cells in Fig. 1. The stationary points for the dynamics generated by the Hamiltonian (8) are defined by the equations,

$$\dot{\theta} = \partial \tilde{H} / \partial I = 0, \quad \dot{I} = -\partial \tilde{H} / \partial \theta = 0,$$

or

$$\frac{\epsilon}{k} (\partial J_l[kr(I)] / \partial I) \cos \theta + \delta\omega = 0, \quad J_l[kr(I)] \sin \theta = 0.$$

Positions of the elliptic stationary points are given by the expressions,

$$\frac{\epsilon}{k} \frac{\partial J_l[kr(I)]}{\partial I} \Big|_{I=I_e} = \mp \delta\omega, \quad \theta_e = 0, \pi, \quad (9)$$

where the sign ‘‘-’’ corresponds to the value of the angle, $\theta_e = 0$, and the sign ‘‘+’’ corresponds to $\theta_e = \pi$. For the positions of the hyperbolic stationary points we have,

$$J_l[kr(I_h)] = 0, \quad \theta_h = \pm \frac{\pi}{2}. \quad (10)$$

As one can see from Eq. (9), in the case of the exact resonance the number of the stable points is infinite. As a consequence, there is an infinite number of the resonance cells. The hyperbolic stable points are connected by the separatrix net, which spans the whole phase space. At the center of each of the cells in this net there is an elliptic stable point (9), and the particle moves around the elliptic points along closed trajectories as shown in Fig. 1.

For a sufficiently large ϵ , chaos destroys the resonant cells as shown in Figs. 2(a), 2(b) in the variables (X, P) , and Figs. 3(b), 3(c) in the variables $[kr(I), \theta]$ for the case $l=1$. However, influence of chaos on the cells is not equal for all cells: the cells with small values of kr are more destroyed than the cells with large values of kr .

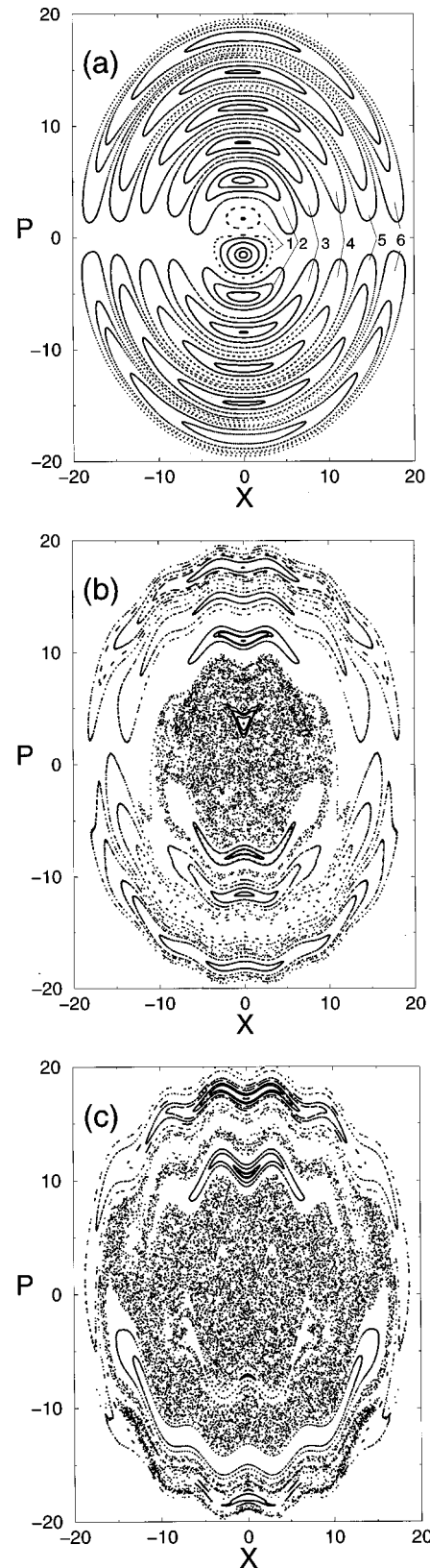


FIG. 2. Resonance cells in the phase space in the coordinates (X, P) for $l = 1$ and (a) $\epsilon=0.5$, the cells are labeled by numbers from 1 to 6; (b) $\epsilon=5$; (c) $\epsilon=10$.

III. QUANTUM DYNAMICS FOR THE EXACT RESONANCE CASE

Let us consider influence of chaos on the dynamics in the quantum model of a harmonic oscillator interacting with

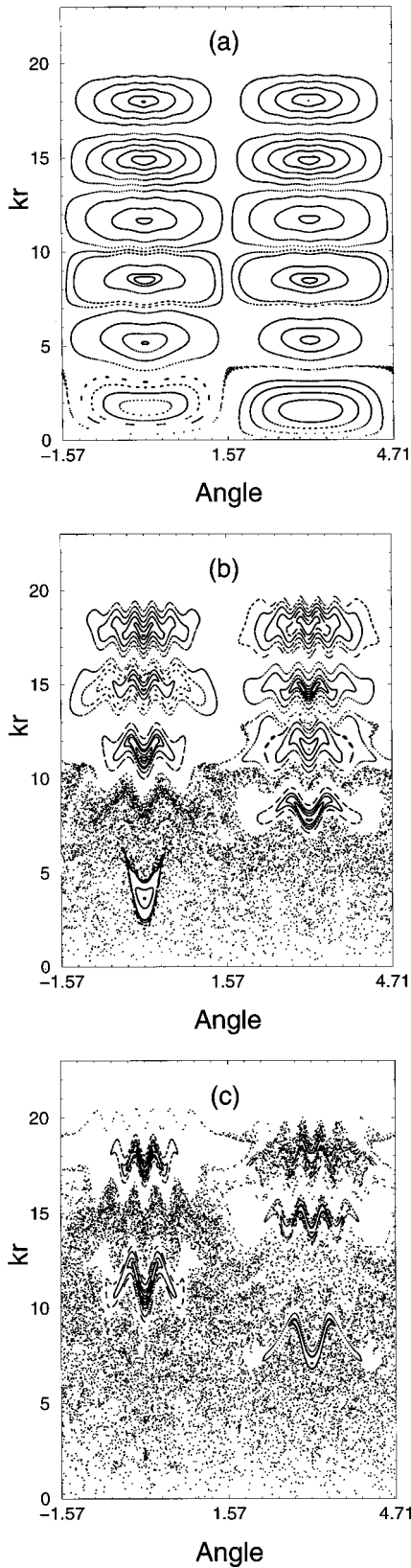


FIG. 3. The resonance cells in the phase space in the coordinates (I, θ) for $l=1$ and (a) $\epsilon=0.5$, (b) $\epsilon=5$, (c) $\epsilon=10$.

the monochromatic wave when the condition of the resonance $\Omega=l\omega$ is satisfied. The quantum Hamiltonian is

$$\hat{H} = \frac{\hat{p}^2}{2M} + \frac{M\omega^2}{2}x^2 + \frac{\epsilon}{k}\cos(kx - \Omega t) = \hat{H}_0 + \hat{V}(x, t), \quad (11)$$

where we use the same notation as in Eq. (1). Since the Hamiltonian (11) is periodic in time, we use the Floquet theorem, and write the solution of the Schrödinger equation in the form

$$\psi_q(x, t) = \exp(-ie_q t/\hbar)u_q(x, t), \quad (12)$$

where \hbar is the Planck constant, e_q is the quasienergy, $\psi_q(x, t)$ is the quasienergy (QE) function, and $u_q(x, t+T) = u_q(x, t)$, with $T=2\pi/\Omega$.

It is convenient to expand the QE functions, $\psi_q(x, t)$, in the complete set of harmonic oscillator eigenstates,

$$\psi_q(x, t) = \exp(-ie_q t/\hbar) \sum_{n=0}^{\infty} C_n^q(t) \psi_n(x), \quad (13)$$

where the expansion coefficients, $C_n^q(t) = C_n^q(t+T)$, are the QE functions in the harmonic oscillator representation. To find the QE states, we used the following numerical procedure.¹³⁻¹⁵ The QE states are the eigenstates of the evolution operator, $\hat{U}(T)$, for one period, T , of the wave field. In order to construct the matrix, $U_{nm} = \langle n | \hat{U}(T) | m \rangle$, of the operator $\hat{U}(T)$, we choose the representation of the Hamiltonian \hat{H}_0 . Applying the evolution operator, $\hat{U}(T)$, to the wave function $\psi(x, 0)$, we have,

$$\hat{U}(T)\psi(x, 0) = \psi(x, T). \quad (14)$$

Next, we choose the initial state in the form: $C_n(0) = \delta_{n, n_0}$. In this way we obtain a column in the evolution operator matrix,

$$U_{n_0, n} = C_n^{(n_0)}(T), \quad (15)$$

where the coefficients, $C_n^{(n_0)}(T)$, can be obtained by numerical solution of the Schrödinger equation (the form of the quantum equations of motion see in Ref. 16). The values of matrix elements, $U_{n, m}$, depend on three dimensionless parameters: the dimensionless wave amplitude, $\epsilon = \epsilon/(k\hbar\omega)$, the quantum parameter, $h = k^2\hbar/M\omega$, which can be treated as a dimensionless Planck constant, and the ratio $\Omega/\omega = l - \delta$. After diagonalization of $U_{n, m}$, we obtain the QE functions, $C_n^q \equiv C_n^q(mT)$, $m=0, 1, 2, \dots$, and the quasienergies, e_q . The QE states can be used to find the state of the quantum system after an arbitrary integer number of periods, mT . We have

$$C_n(mT) = \sum_{n'} C_{n'}(0) \sum_q C_{n'}^{q*} C_n^q \exp(-ie_q mT/\hbar), \quad (16)$$

where the coefficients, $C_{n'}(0)$, are the amplitudes of the probability distribution at the initial moment, $t=0$.

In the resonance approximation, the QE functions, $C_n^q(t)$, are independent of time and satisfy the system of algebraic equations,¹⁶

$$(E_q - \delta n)C_n^q = \frac{\epsilon}{\hbar}(V_{n, n+1}C_{n+1}^q + V_{n, n-1}C_{n-1}^q), \quad (17)$$

where $E_q = e_q/\hbar\omega$ is the dimensionless quasienergy. In this section, we study the case of exact resonance, when $\delta=0$. The off-resonant case will be considered in the next section.

The matrix elements in Eq. (17) have the form,¹⁶

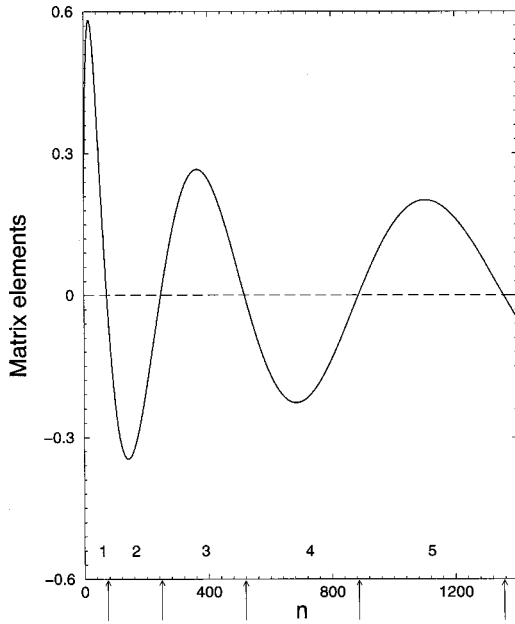


FIG. 4. The matrix elements, $2V_{n,n+1}$, vs. n . The resonance cells are labeled by numbers from 1 to 5. The arrows indicate the boundaries, $b_{i,i+1}$, between i th and $i+1$ th cells ($b_{1,2}=73$, $b_{2,3}=247$, $b_{3,4}=518$, $b_{4,5}=888$, $b_{5,6}=1357$); $l=1$, $h=0.1$.

$$V_{n,n+2m+1} = \frac{(-1)^m h^m e^{-h/4}}{2^{m+1} \sqrt{(n+1) \cdots (n+2m+1)}} L_n^{2m+1} \left(\frac{h}{2} \right), \quad (18a)$$

$$V_{n,n+2m} = \frac{(-1)^m h^m e^{-h/4}}{2^{m+1} \sqrt{(n+1) \cdots (n+2m)}} L_n^{2m} \left(\frac{h}{2} \right), \quad (18b)$$

where L_n^m are the Laguerre polynomials. For $n \gg 1$, the matrix element can be expressed in terms of the Bessel functions, J_m ,

$$V_{n,n+2m+1} = \frac{1}{2} \frac{(-1)^m n^{m+1/2} e^{-h/4}}{\sqrt{(n+1) \cdots (n+2m+1)}} J_{2m+1}(\sqrt{2nh}), \quad (19a)$$

$$V_{n,n+2m} = \frac{1}{2} \frac{(-1)^m n^m e^{-h/4}}{\sqrt{(n+1) \cdots (n+2m)}} J_{2m}(\sqrt{2nh}). \quad (19b)$$

One can see that matrix elements, $V_{n,n+l}$, in Eq. (17) oscillate as a function of n . In particular, for $l=1$, they can be expressed in terms of the Bessel function, $J_1(\sqrt{2nh})$,

$$V_{n,n+1} = \frac{1}{2} \sqrt{\frac{n}{n+1}} \exp\left(-\frac{h}{4}\right) J_1(\sqrt{2nh}). \quad (20)$$

Here the argument of the Bessel function in the quantum model is the quantized dimensionless radius, $kr_n = \sqrt{2nh}$. When the transition probability, $V_{n,n+1}$, in Eq. (17) is small, the boundaries of quantum resonance cells are defined by the zeros of the Bessel function, $J_1(\sqrt{2nh})$. In Fig. 4, the matrix elements, $V_{n,n+1}$, are plotted as a function of n , and the boundaries of the resonant cells are marked by arrows. In the quasiclassical limit, when $n \rightarrow \infty$, $h \rightarrow 0$, $I/I_0 = hn$ ($I_0 = M\omega/lk^2$), the boundaries of the quantum cells, defined by the zeros of the Bessel function, $J_1(\sqrt{2nh})$, in Eq. (20) co-

incide with the boundaries of the classical cells, defined by zeros of the Bessel function in Eq. (10).

Due to oscillations of the matrix elements with n , the three-diagonal system (17) breaks up into relatively independent blocks. As a consequence, the most part of the QE functions are localized inside one of the quantum cells. To show this, let us characterize each QE function by its average, $n_q = \sum_n n |C_n^q|^2$ and its dispersion, $\sigma_q = [\sum_n (n - n_q)^2 |C_n^q|^2]^{1/2}$. The plot, $n_q = n_q(\sigma_q)$, is shown in Figs. 5(a)–5(c) for three values of ϵ . Each QE function on the diagram is represented by a single point. One can see that the QE functions are localized inside the cells [boundaries of the cells in Figs. 5(a)–5(c) are marked by arrows], because the averages of these QE functions are located inside the cells, and their dispersions are less than the distance to the boundary of the cell. Each group of states localized in one cell forms a row in these plots. Besides the localized QE functions, there exist delocalized QE states which are represented by scattered points with large dispersion, σ_q . These QE states provide the diffusion of the particle between the resonant cells. From comparison of Fig. 5(b) with Fig. 5(a), one can see that an increase of ϵ from 1 to 2 results in decrease in the number of the delocalized states. The effect of localization of the quantum delocalized states under influence of chaos was studied in Ref. 15. When we further increase ϵ , from $\epsilon=2$ to $\epsilon=3$ [see Fig. 5(c)], the number of the delocalized states increases again. One can see from Fig. 5(b) that the localized QE states split into two groups: the QE states in one group interact with the QE states of the next cells and shift up; the QE states in the other group shift down due to interaction with the QE states of the preceding cell. As shown in Fig. 5(b), the QE states of the first two cells, at $\epsilon=2$, strongly interact; and at $\epsilon=3$ the boundary between the first and second cells disappears. This corresponds to chaotization of the first two cells in classical phase space.

A dynamical manifestation of the division of the Hilbert space into quantum resonance cells is the effect of localization of the quantum states within the cells. In other words, if the initial state is chosen in some resonance cell, then it remains localized inside this initial cell. In the left side of Figs. 6(a)–6(c) the probability distribution at the time $t = 1000T$, is shown, for three values of ϵ . The right side shows the classical phase space for the same parameters. The arrows indicate the boundaries of the cells. The initial distribution, indicated in Fig. 6(a) by the dashed line, was: $C_n(0) = \exp(-n/\delta n)$, with $\delta n = 20$. This particular form of the initial distribution can be associated with a finite temperature of the system.

Let us present the initial probability distribution as: $P_n(0) = |C_n(0)|^2 = \exp(-\hbar\omega n/\tau)$, where τ is the temperature measured in energy units. In dimensionless units, this expression can be rewritten as: $P_n(0) = \exp(-hn/\Theta)$, where the dimensionless temperature, $\Theta = \tau/(M\omega^2/k^2)$, is measured in the same units as the wave amplitude, ϵ . The value $\delta n = \Theta/h = 20$ at $h=0.1$, which was chosen in our simulations, corresponds to the dimensionless temperature, $\Theta=2$. For ionized calcium with $M = 6.64 \times 10^{-23}$ g, $\omega = 2\pi \times 500$ kHz, and $k = 1.58 \times 10^5$ cm $^{-1}$, the value $\Theta=2$ corresponds to the temperature of 5×10^{-4} K.

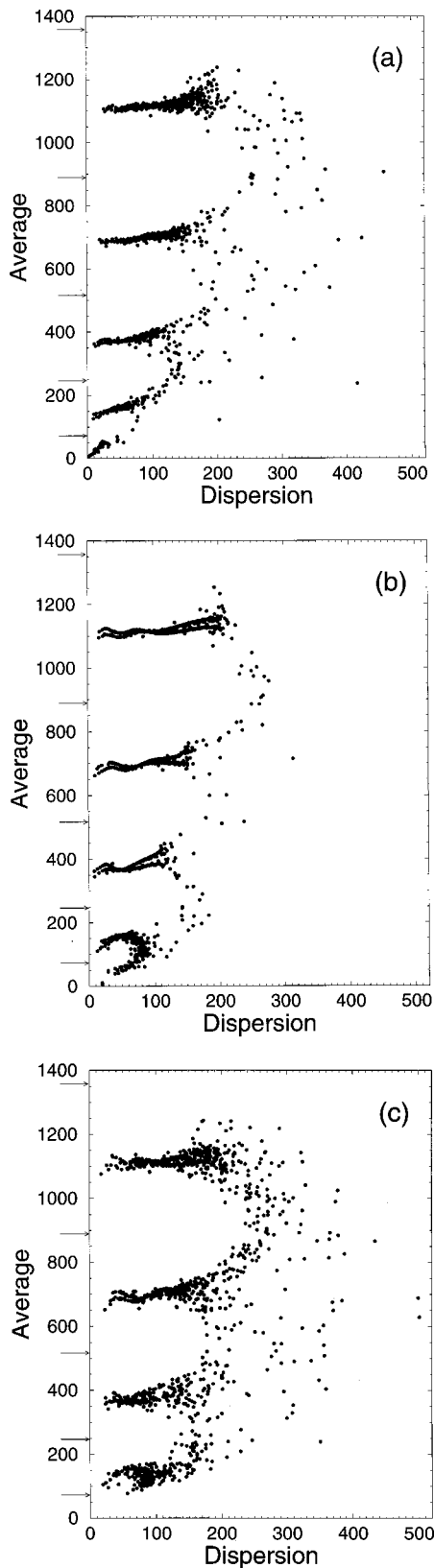


FIG. 5. The averages, n_q , of QE functions vs. their dispersions, σ_q , for three values of the wave amplitude, (a) $\epsilon=1$, (b) $\epsilon=2$, (c) $\epsilon=3$; $l=1$, $h=0.1$.

As one can see from the left side of Fig. 6(a), almost all of the initial distribution function is located in the first cell, and remains localized within the initial cell in subsequent times, when the value of ϵ is small enough ($\epsilon=1$). With

increasing ϵ ($\epsilon=2$) in Fig. 6(b), the second classical cell [right side in Fig. 6(b)] becomes chaotic and as a consequence the boundary between the first and the second cells in the left side in Fig. 6(b) disappears, and the probability, $|C_n(t)|^2$, becomes almost independent of whether n is located in the first or in second cell. A further increase of ϵ [in left side in Fig. 6(c)] up to the value $\epsilon=3$, leads to an increase of the probability in the cells with large values of n by a few orders-of-magnitude.

For experimental investigation of quantum chaos we propose to use the property of localization in quantum cells, initially explored in Ref. 9. As one can see on the left side in Figs. 6(a)–6(c), the average probability distribution as a function of n remains approximately the same inside the cells, and changes only at the boundaries of the cells. Let us define the cell's probability, P_i , as the probability of finding the particle in the i th cell. We have: $P_i = \sum_{n_i}^{n_{i+1}} |C_n(t)|^2$, where n_i and n_{i+1} are the boundaries of i th and $i+1$ th cells in the Hilbert space. In Figs. 7(a)–7(c) the probabilities P_i are shown as a function of time, $m=t/T$, for the same values of ϵ as in Figs. 5(a)–5(c), 6(a)–6(c). One can see that after a transition period, a cell's average probability remains independent of time.

When the first two classical cells on the right side in Fig. 6(c) become chaotic, the quantum probability redistributes approximately uniformly between the corresponding quantum cells shown on the left side in Fig. 6(c). In Fig. 7(c), P_2 is larger than P_1 , because the number of levels in the second cell is larger than the number of levels in the first cell. The average relative probabilities are $P_1/n_1 \approx 4.1 \times 10^{-3}$ and $P_2/n_2 \approx 3.3 \times 10^{-3}$.

Since the average cell probabilities do not change with time, it is reasonable to average them. Time-averaged probabilities \bar{P}_i as a function of the wave amplitude, ϵ , are presented in Fig. 8. It is possible to use the dependence shown in Fig. 8 for comparison with experimental results, namely, to measure the probability of finding a particle not on a given level, n , but in a given cell, i .

The numerical approach based on using the QE states for computing the dynamics by Eq. (16) is very convenient, because it allows one to determine the state of the system by a simple summation. This procedure makes it possible to average the quantum quantities over large time intervals. We compared the average energy and the dispersion of energy for the chaotic classical system and for the corresponding quantum system. The quantum average energy and the dispersion of energy can be measured experimentally. The results are presented in Figs. 9 and 10. One can see from Figs. 9 and 10 that the average energy and dispersion in the quantum and classical models are approximately the same. The quantum data are presented for two values of the dimensionless Planck constant, $h=0.1$ and $h=1$. One can see that the value of h does not affect significantly the chaotic dynamics, except when the value of ϵ is small enough, $\epsilon < 2$. In this region, an increase in h results in an increase in the number of the delocalized states [represented by scattered points with large dispersions in Fig. 5(a)]. As a consequence, the diffusion rate in Figs. 9 and 10 increases with h increasing. The average in the quantum model at large values of ϵ ($\epsilon > 8$ in

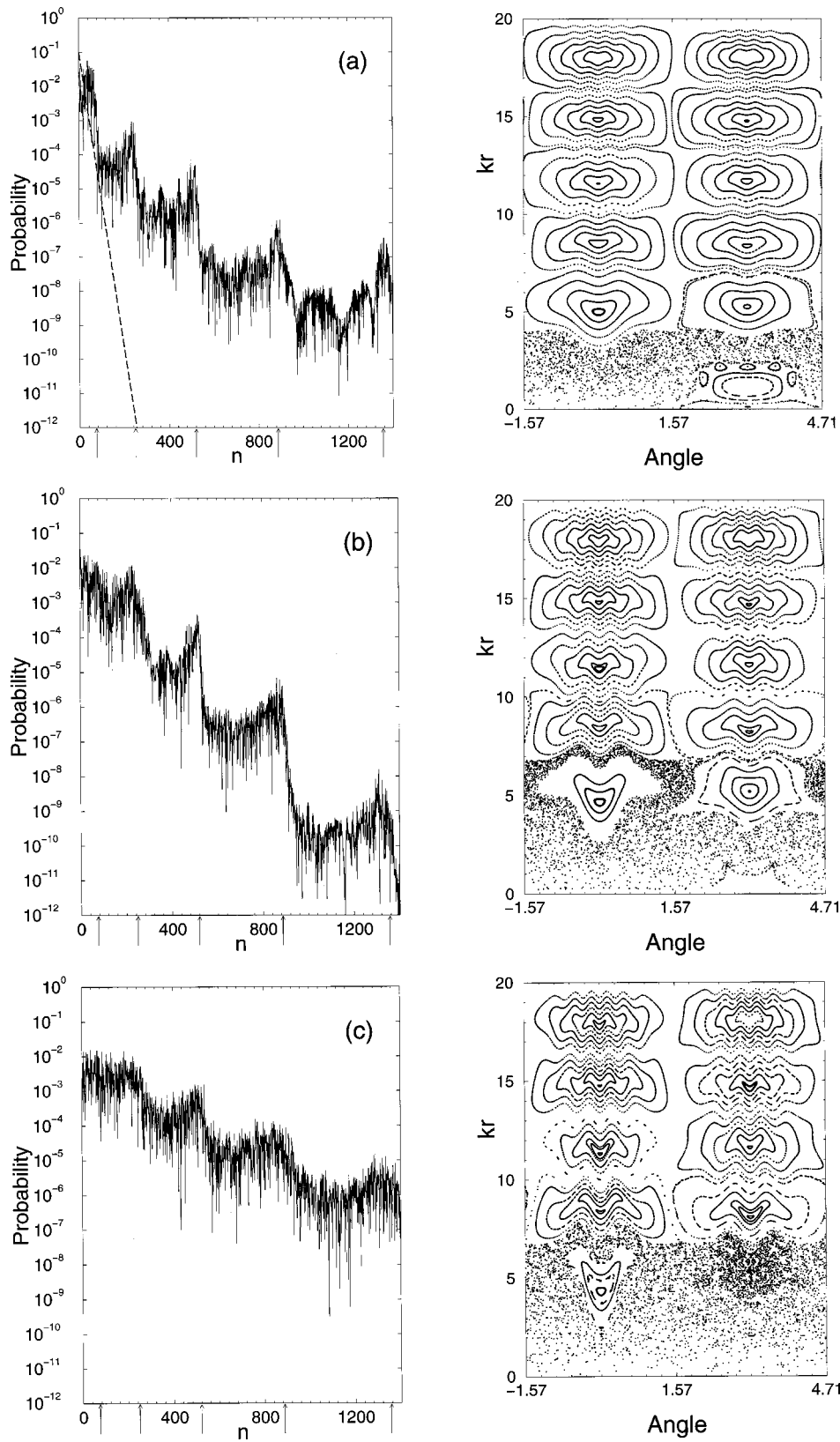


FIG. 6. Left side: the probability distribution at the time, $t = 1000T$, for $h = 0.1$, $l = 1$ and (a) $\epsilon = 1$, (b) $\epsilon = 2$, (c) $\epsilon = 3$. The initial distribution is illustrated by the dashed line. Right side: the classical phase space for the same parameters.

Fig. 9) is less than the average in the classical model. This difference does not represent any physical effect, and is a consequence of the artificial truncation of the Hilbert space: the quantum Hilbert space used in the calculations is finite, while the classical phase space is infinite.

IV. QUANTUM DYNAMICS IN THE NEAR-RESONANCE CASE

In the preceding section we considered the chaotic dynamics for the case of exact resonance. A more common

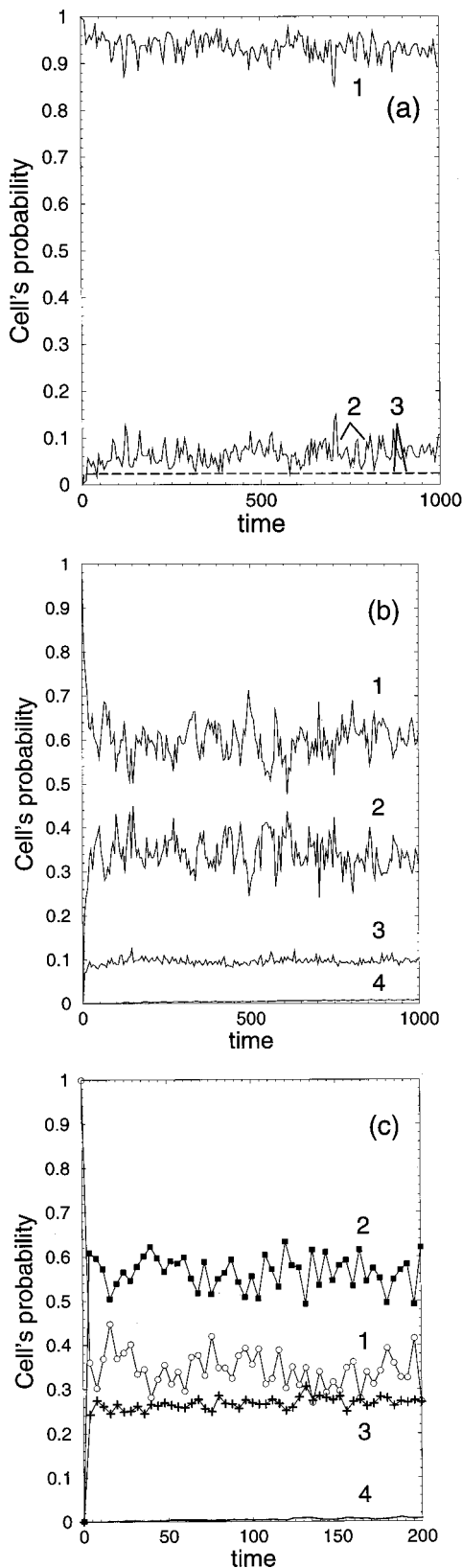


FIG. 7. Time-evolution of the probability of finding a particle in the i th cell. The cells are labeled by the numbers from 1 to 4; $h=0.1$, $l=1$; (a) $\epsilon=1$, solid lines: $i=1,2$, dashed line: $i=3$; (b) $\epsilon=2$, (c) $\epsilon=3$, circles: $i=1$, squares: $i=2$, crosses: $i=3$, no symbols: $i=4$.

situation occurs when the frequencies of the wave and the oscillator do not satisfy exactly the resonance condition, i.e., when $\delta=l-\Omega/\omega \neq 0$. In this case, in the classical phase space there exists a finite number of the resonance cells,

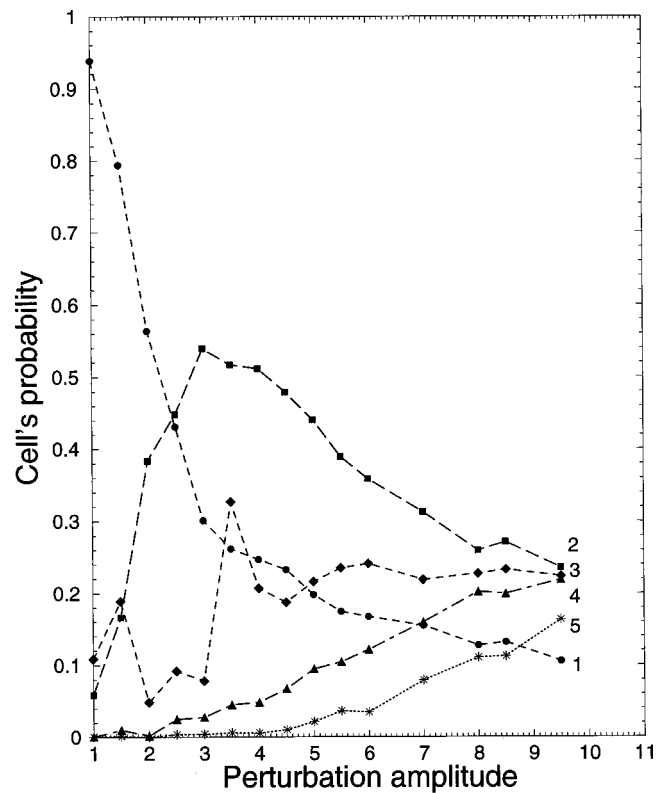


FIG. 8. Time-averaged probability distribution to find a particle in the individual cells, the cells are labeled by numbers, from 1 to 5. The averaging was performed in the time interval: $t=2000-12\,000T$, over 50 points, $h=0.1$, $l=1$.

because Eq. (9) is satisfied for a finite number of the stable points, $kr(I_e)$. When $\delta \neq 0$, the infinite separatrix in the classical phase space is destroyed. As a consequence, in the quantum system one may anticipate that the separatrix QE states are destroyed, too. Since the separatrix QE states provide tunneling between the cells, their destruction should result in localization of the quantum states. In Fig. 11(a) we plot, $n_q(\sigma_q)$ for the near-resonance case, when $\delta=0.01$, and for small ϵ . In Fig. 11(b) the probability distribution at time $t=10^4T$ is shown and in Fig. 11(c) the phase space for the same parameters as in Figs. 11(a) and 11(b) is illustrated. One can see from Fig. 11(a) that when $\delta \neq 0$, there are no delocalized QE functions with large dispersion, as, for example, in Fig. 5(a). This is different from the case of the exact resonance, when the separatrix QE states exist at arbitrarily small ϵ .¹⁵ As a consequence, there is no tunneling between the cells and a quantum state, localized in some region of the Hilbert space, remains localized in the initial region for any time, as shown in Fig. 11(b). Quantum localization is the quantum manifestation of localization of classical trajectories in the phase space. At small ϵ , there is only one resonance cell in the classical phase space, as shown in Fig. 11(c), the stochastic web is absent, the particle is localized, and cannot travel along the web.

One can see from Fig. 11(a) that QE states in central regions corresponding to resonant cells are more delocalized than those near the separatrices. In order to treat this property, let us compare the plot of $n_q(\sigma_q)$ with the corresponding classical phase space. Each value of n in the quantum

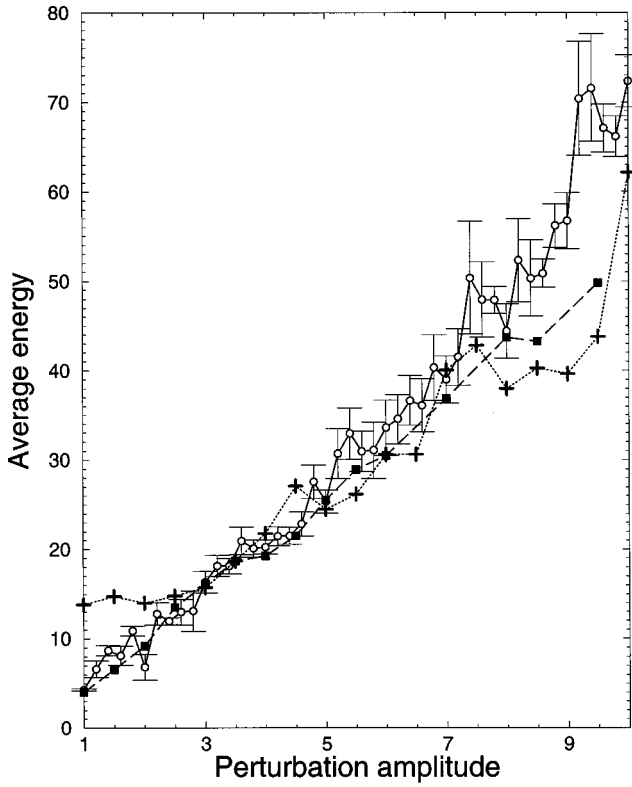


FIG. 9. Time-averaged value of the energy, $\bar{E}_{\text{quant}} = h(\bar{n}_{\text{quant}} + 1/2)$, where $\bar{n}_{\text{quant}} = \sum_{i=1}^{N_{\text{quant}}} \bar{n}_i / N_{\text{quant}}$, $n_i = \sum_n n |C_n(t_i)|^2$ for the quantum model; and for the classical model: $\bar{E}_{\text{cl}} = \bar{\rho}^2/2$, where $\bar{\rho}^2 = \sum_{i=1}^{N_{\text{cl}}} \rho^2(t_i) / N_{\text{cl}}$. In the quantum model, averaging was performed in the time interval: $t = 2000T$ to $12\,000T$ over $N_{\text{quant}} = 50$ points. In the classical model, averaging was performed over 15 chaotic trajectories in the time interval: $t = 50T$ to $15\,050T$ ($N_{\text{cl}} = 15\,000$); the solid line and circles indicate classical results; the dashed line and squares indicate quantum results for $h = 0.1$; the dotted line and crosses indicate quantum results for $h = 1$; $l = 1$. The error bars for the quantum results are of the size of the symbols.

system corresponds to a quantized classical action, $I_n/I_0 = nh$, where $I_0 = M\omega/lk^2$, or to the quantized dimensionless radius, $kr_n = \sqrt{2n\hbar}$. Each value of action I_n (or kr_n) corresponds to the set of classical trajectories. Moving along the trajectory the particle can approach the values of I_n in the interval $I_{n_1} < I_n < I_{n_2}$. The corresponding QE state will be delocalized over the states with the numbers n in the interval $n_1 < n < n_2$. The more curved the trajectory in the phase space is, the more spread is the QE state corresponding to this trajectory in the quantum case. In the classical phase space in Fig. 11(c) the least curved trajectories correspond to the actions (radii) satisfying the condition (10). As the consequence, the quantum states near the point $hn_h = I_h/I_0$ (here subscript means ‘‘hyperbolic,’’ and h in the denominator means the dimensionless Planck constant, $h = k^2\hbar/M\omega$) have the smallest dispersions.

Modification of the QE states, and modification of the classical and quantum dynamics at increasing the wave amplitude, ϵ , in the near resonance case is shown, respectively, in Figs. 12(a)–12(c) and 13(a)–13(c). As one can see from Figs. 12(a)–12(c), the QE states quickly become delocalized as ϵ increases. The delocalization of the QE functions is caused by two processes. The first is the formation of quan-

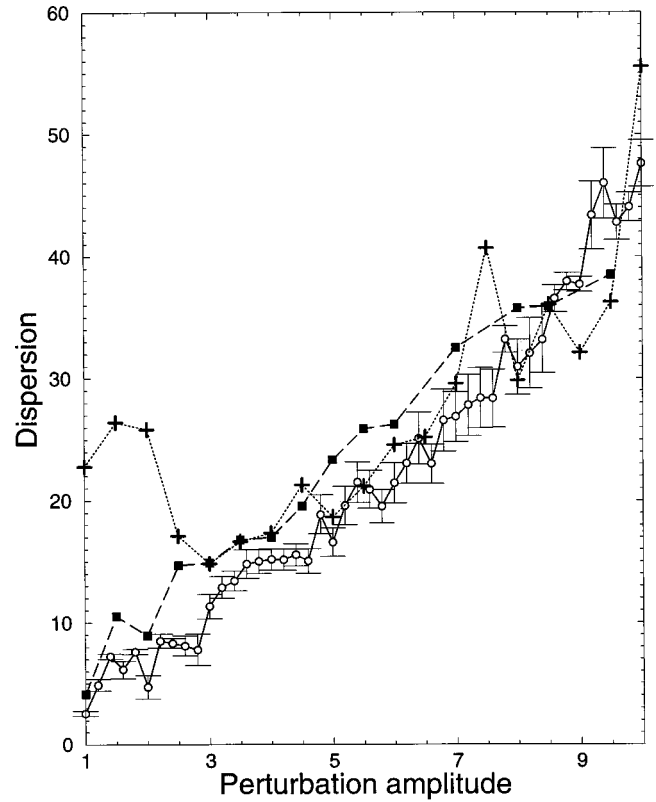


FIG. 10. Time-averaged value of the dispersion of the energy, $\overline{\Delta E}_{\text{quant}} = h\bar{\sigma}_{\text{quant}}$, where $\bar{\sigma}_{\text{quant}} = \sum_{i=1}^{N_{\text{quant}}} \sigma_i / N_{\text{quant}}$, $\sigma_i = \sqrt{\sum_n (n - \bar{n}_i)^2 |C_n(t_i)|^2}$ for the quantum model; and for the classical model: $\overline{\Delta E}_{\text{cl}} = \{\sum_{i=1}^{N_{\text{cl}}} [\rho(t_i)^2/2 - \bar{\rho}^2/2]^2 / N_{\text{cl}}\}^{1/2}$. In the quantum model, averaging was performed in the time interval $t = 2000$ – $12\,000T$ over $N_{\text{quant}} = 50$ points. In the classical model, averaging was performed over 15 chaotic trajectories in the time interval $t = 50$ – $15\,050T$, ($N_{\text{cl}} = 15\,000$); the solid line and circles indicate classical results; the dashed line and squares indicate quantum results for $h = 0.1$; the dotted line and crosses indicate quantum results for $h = 1$; $l = 1$. The error bars for quantum results are of the size of the symbols.

tum resonance cells [see Ref. 9, Eq. (8)] as ϵ increases. This corresponds to formation of classical resonance cells in phase space, defined by the condition (9). The second process, which leads to delocalization of the quantum states, is chaotization of the classical dynamics. These two phenomena can be observed on the right side in Fig. 13(a). The dynamics at $\epsilon = 1$ in the region near the first cell is mostly chaotic, while the sixth cell (at $\theta = \pi/2$) is not yet formed.

Similar features can be observed in the quantum dynamics. One can see from Fig. 11(b) that when ϵ is small, the perturbation mostly affects the first two cells, while the probability distribution in the third, fourth, and fifth cells almost coincides with the probability distribution for the initial state. The same features can be observed in the classical phase space in Fig. 11(c). Further increase of ϵ , up to $\epsilon = 1$, affects the quantum and classical dynamics in all cells, as shown in Fig. 13(a). The number of the resonant cells in the classical phase space increases [see Eq. (9)], and the Hilbert space on the left side in Fig. 13(a) begins to divide into cells, too. One can see the formation of characteristic plateaus in the probability distribution. When $\epsilon = 2$ the plateaus in the probability distribution on the left side in Fig. 13(b) become more discernible. In the classical phase space, for the corresponding

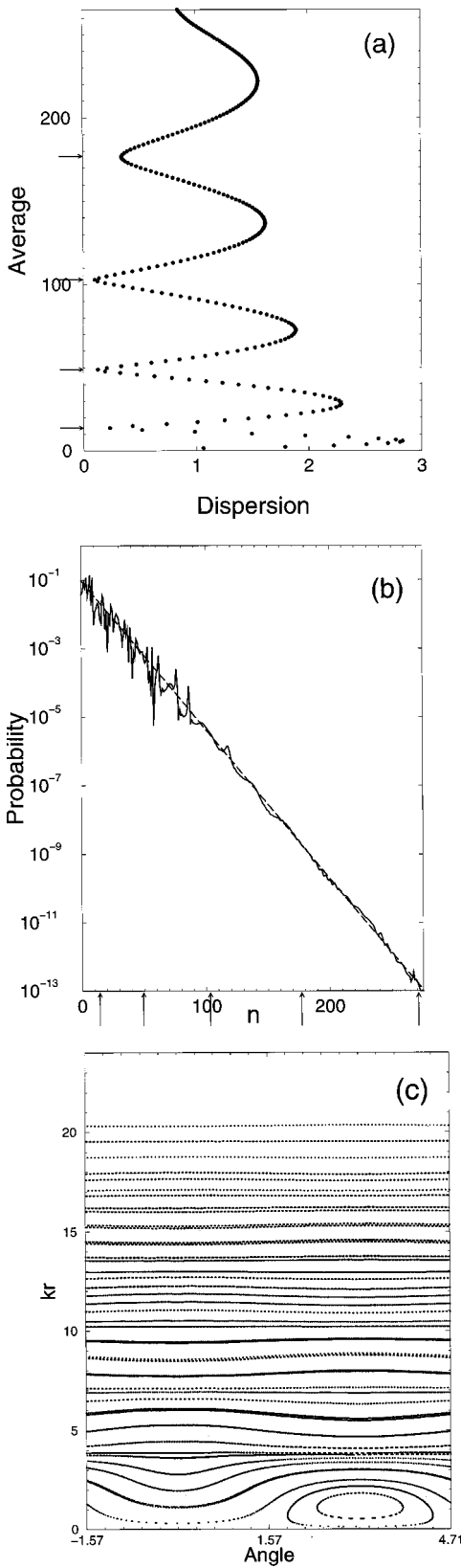


FIG. 11. (a) Averages, n_q , of QE functions versus their dispersions, σ_q , (b) the quantum probability distribution at time $t = 10^4 T$, and (c) the classical phase space; $l = 1$, $\epsilon = 0.05$, $h = 0.5$, $\delta = 0.01$. The boundaries of the cells (for the corresponding resonance case) are marked by arrows.

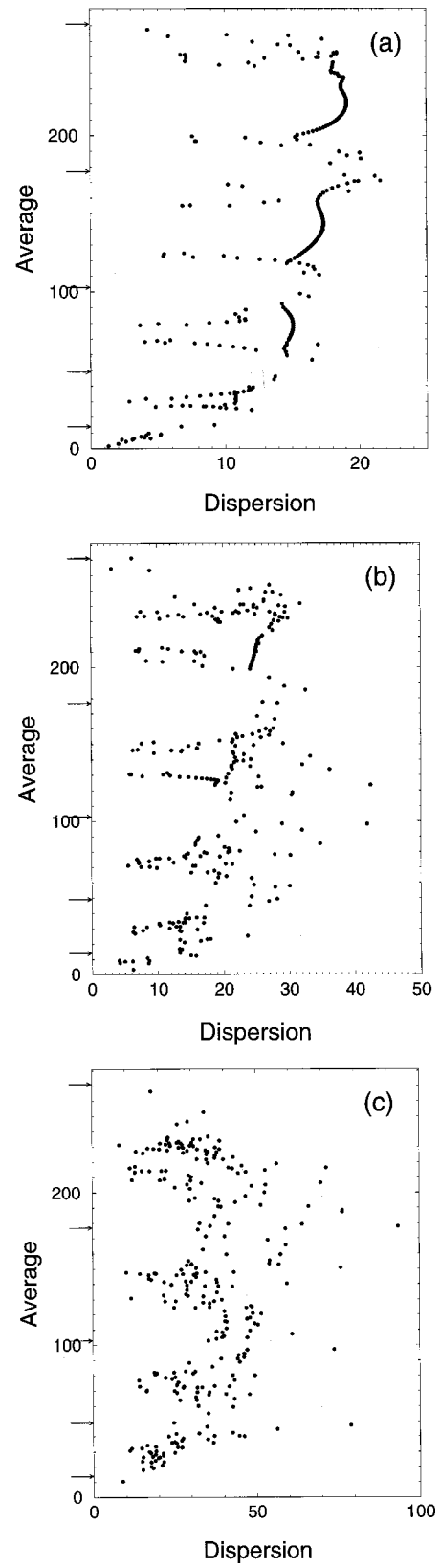


FIG. 12. Averages, n_q , of the QE functions vs. their dispersion, σ_q , for three values of the wave amplitude, ϵ , (a) $\epsilon = 1$, (b) $\epsilon = 2$, (c) $\epsilon = 3$, in the near resonance case, when $\delta = 0.01$; $l = 1$, $h = 0.5$. The boundaries of the corresponding resonance cells are marked by arrows.

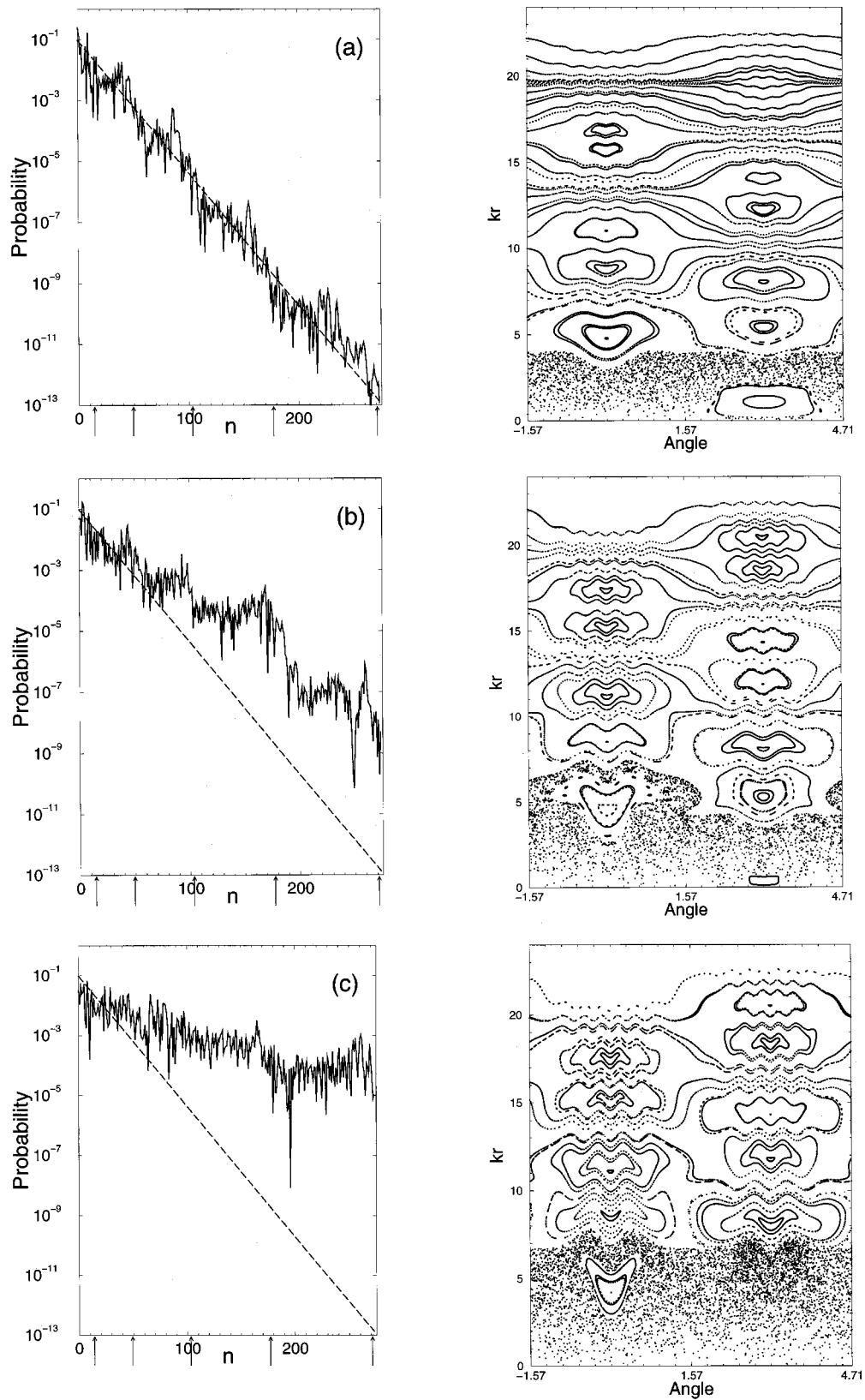


FIG. 13. Left side: the probability distribution at the time, $t = 10^4 T$, for $h = 0.5$, $l = 1$, $\delta = 0.01$ and (a) $\epsilon = 1$, (b) $\epsilon = 2$, (c) $\epsilon = 3$. The initial distribution is indicated by the dashed line. Right side: the classical phase space for the same parameters.

parameters, the area of resonance cells also increases. Comparison of Figs. 5(a)–5(c) with Figs. 12(a)–12(c), and Figs. 6(a)–6(c) with Figs. 11(b), 11(c), 13(a)–13(c) allows us to conclude that the influence of detuning, δ , on the dynamics

becomes less significant when the ratio ϵ/δ increases, which can be seen from the structure of Eqs. (8) and (17) (see also Ref. 9). Thus, the structure of the probability distribution in the left side of Fig. 13(a) differs qualitatively from those in

Fig. 6(a), while the left sides of Figs. 13(c) and 6(c) are similar. The same can be said about classical dynamics when we compare Fig. 13(a) with Fig. 6(a) and Fig. 13(c) with Fig. 6(c).

V. CONCLUSION

In conclusion, we have investigated the transition to quantum chaos of a trapped ion interacting with two laser fields with slightly different frequencies. We compared the classical and quantum dynamics in this system. Our approach to the quantum problem is based on the quasienergy states. It was shown that the Hilbert space of the quantum system is reasonable to separate into quantum resonance cells—similar to the resonance cells in the classical phase space—and to measure the average quantum probability in each cell. This technique will allow one to simplify the measurement of the probability distribution, because in this case it is not necessary to measure the probability at a fixed oscillator state, n . It is enough to measure the probability distribution in the interval $n_i < n < n_{i+1}$, where n_i and n_{i+1} are the boundaries between the i th and the $i+1$ th quantum resonance cells. The locations of the boundaries of the quantum resonance cells in Hilbert space, in the quasiclassical limit, correspond to the locations of the separatrices in the classical phase space.¹⁶

The average energy, \bar{E} , and the dispersion of energy, $\bar{\sigma}$, are calculated in both the quantum and the classical cases. It is shown that \bar{E} and the dispersion, $\bar{\sigma}$, in the quantum and classical systems are approximately the same. It is interesting to compare this result with the results obtained for other dynamical systems. The system studied in this article in the exact resonance case possesses the inhomogeneous stochastic web. The web width decreases when r (or I) increases, so that the classical diffusion is practically limited. The results for quantum chaotic dynamics in the system with inhomogeneous stochastic web obtained in this article differ from the results obtained for the quantum chaotic dynamics in the systems where the classical diffusion is unlimited, such as kicked rotor¹⁰ or kicked oscillator.¹¹ It was shown that the dynamics in the two latter systems repeat the classical dynamics only during a finite time, $t < t_0$ after which the quantum interference effects limit the quantum diffusion. Due to the results of this article, the dynamics in the system with limited classical diffusion in the regime of strong classical chaos is independent of the quantum parameter \hbar , and the chaotic dynamics in the quantum and classical systems on average coincides for any time, t . This feature differentiates the studied system from the kicked systems mentioned above.

The influence of finite detuning, $\delta \neq 0$, is analyzed for both quantum and classical cases. It is shown that for a small amplitude, ϵ , the condition, $\delta \neq 0$, considerably affects the dynamics: the resonance cells disappear (for the classical case, see also Ref. 18), and the quantum and classical states are localized. (In the classical case, the term “localization” means here that $I \sim \text{const}$. In the quantum case, it means that the probability distribution exponentially decreases with the distance from the initial state.) For $\epsilon \gg \delta$, there are cells (for

small kr), where the dynamics, in the case $\delta \neq 0$, is similar to that for exact resonance, when $\delta = 0$. The character of the localization of quantum states, when ϵ increases and $\delta \neq 0$, also changes. When ϵ is small, we observe the exponential localization characteristic for nondegenerate system. In this case, the probability exponentially decreases with the distance from the initial state. For $\epsilon \gg 1$, we observe the localization over the cells, characteristic for the degenerate system, when the probability distribution decreases exponentially only at the boundaries of the quantum cells, being on average the same in the central regions of the cells. The transition from one type of localization to another is the quantum manifestation of transition from the classical dynamics characteristic for the nondegenerate system to the classical dynamics characteristic for the degenerate system (for discussion of the transition in the classical system see, for example, Refs. 12, 19).

ACKNOWLEDGMENTS

This work was supported by the Department of Energy under the contract W-7405-ENG-36, and by the National Security Agency. Work of D.I.K. was partly supported by Russian Foundation for Basic Research (Grants No. 98-02-16412 and 98-02-16237).

¹C. Monroe, D. M. Meekhof, B. E. King, and D. J. Wineland, *Science* **272**, 1131 (1996).

²D. J. Wineland, C. Monroe, D. M. Meekhof, B. E. King, D. Leibfried, W. M. Itano, J. C. Bergquist, D. Berkeland, J. J. Bollinger, and J. Miller, *Proc. R. Soc. London, Ser. A* **454**, 411 (1998).

³M. Roberts, P. Taylor, G. P. Barwood, P. Gill, H. A. Klein, and W. R. C. Rowley, *Phys. Rev. Lett.* **78**, 1876 (1997); D. J. Berkeland, J. D. Miller, J. C. Bergquist, W. M. Itano, and D. J. Wineland, *ibid.* **80**, 2089 (1998).

⁴R. J. Hughes, D. F. V. James, J. J. Gomez, M. S. Gulley, M. H. Holzschteiter, P. G. Kwiat, S. K. Lamoreaux, C. G. Peterson, V. D. Sandberg, M. M. Schauer, C. M. Simmons, C. E. Thorburn, D. Tupa, P. Z. Wang, and A. G. White, *Fortschr. Phys.* **46**, 329 (1998).

⁵J. I. Cirac and P. Zoller, *Phys. Rev. Lett.* **74**, 4091 (1995); C. Monroe, D. M. Meekhof, B. E. King, W. M. Itano, and D. J. Wineland, *ibid.* **75**, 4714 (1995).

⁶S. A. Gardiner, J. I. Cirac, and P. Zoller, *Phys. Rev. Lett.* **79**, 4790 (1997).

⁷A. J. Scott, C. A. Holmes, and G. J. Milburn, *Phys. Rev. A* **61**, 013401 (2000).

⁸G. P. Berman, D. F. V. James, R. J. Hughes, M. S. Gulley, M. H. Holzschteiter, and G. V. López, *Phys. Rev. A* **61**, 023403 (2000).

⁹V. Ya. Demikhovskii and D. I. Kamenev, *Phys. Lett. A* **228**, 391 (1997).

¹⁰G. Casati, B. V. Chirikov, J. Ford, and F. M. Izrailev, *Lect. Notes Phys.* **93**, 334 (1979).

¹¹I. Dana, *Phys. Rev. Lett.* **73**, 1609 (1994).

¹²G. M. Zaslavsky, R. Z. Sagdeev, D. A. Usikov, and A. A. Chernikov, *Weak Chaos and Quasi-Regular Patterns* (Cambridge University Press, Cambridge, 1992).

¹³G. P. Berman, A. R. Kolovsky, and G. M. Zaslavsky, *Phys. Lett. A* **111**, 17 (1982).

¹⁴L. E. Reichl and W. A. Lin, *Phys. Rev. A* **40**, 1055 (1989).

¹⁵V. Ya. Demikhovskii, D. I. Kamenev, and G. A. Luna-Acosta, *Phys. Rev. E* **59**, 294 (1999).

¹⁶V. Ya. Demikhovskii, D. I. Kamenev, and G. A. Luna-Acosta, *Phys. Rev. E* **52**, 3351 (1995).

¹⁷I. S. Gradshteyn and I. M. Ryzhik, *Table of Integrals, Series and Products* (Academic, New York, 1980).

¹⁸A. J. Lichtenberg and M. A. Leiberman, *Regular and Stochastic Motion* (Springer, New York, 1983).

¹⁹B. V. Chirikov and V. V. Vecheslavov, *The Structure of Weakly Nonlinear Resonance*, preprint of the Institute of Nuclear Physics, Novosibirsk, 1991.